

Robust Nonprehensile Object Transportation with Uncertain Inertial Parameters

Adam Heins and Angela P. Schoellig

Abstract—We consider the nonprehensile object transportation task known as the *waiter’s problem*—in which a robot must move an object balanced on a tray from one location to another—when the balanced object has uncertain inertial parameters. In contrast to existing approaches that completely ignore uncertainty in the inertia matrix or which only consider small parameter errors, we are interested in pushing the limits of the amount of inertial parameter uncertainty that can be handled. We first show how balancing constraints robust to inertial parameter uncertainty can be incorporated into a motion planning framework to balance objects while moving quickly. Next, we develop necessary conditions for the inertial parameters to be realizable on a bounding shape based on moment relaxations, allowing us to verify whether a trajectory will violate the balancing constraints for *any* realizable inertial parameters. Finally, we demonstrate our approach on a mobile manipulator in simulations and real hardware experiments: our proposed robust constraints consistently balance a 56 cm tall object with substantial inertial parameter uncertainty in the real world, while the baseline approaches drop the object while transporting it.

I. INTRODUCTION

The *waiter’s problem* [1] is a nonprehensile manipulation task that requires a robot to transport objects from one location to another while keeping them balanced on a tray at the end effector (EE), like a restaurant waiter. This manipulation task is called *nonprehensile* [2] because the objects are not rigidly grasped: they are only attached to the robot by frictional contact and thus retain some independent degrees of freedom. Other examples of nonprehensile manipulation include pushing, rolling, and throwing [3], [4]. A nonprehensile approach avoids grasping and ungrasping phases and can handle delicate or unwieldy objects which cannot be adequately grasped at all [5]; such an approach for transporting objects is useful in industries including food service, warehouse fulfillment, and manufacturing.

We build on our previous work on the waiter’s problem for mobile manipulators [6]. In contrast to [6], which focused on fast online replanning to react to dynamic obstacles while balancing objects with *known* properties, here we focus on offline planning for a balanced object with *unknown* inertial parameters—that is, the values of the mass, center of mass (CoM), and inertia matrix are not known exactly but rather lie in some set. Our approach is to plan trajectories to reach

The authors are with the Learning Systems and Robotics Lab (www.learnsyslab.org) at the Technical University of Munich, Germany, and the University of Toronto Institute for Aerospace Studies, Canada. They are also affiliated with the University of Toronto Robotics Institute, the Munich Institute of Robotics and Machine Intelligence (MIRMI), and the Vector Institute for Artificial Intelligence. E-mail: adam.heins@robotics.utoronto.ca, angela.schoellig@tum.de

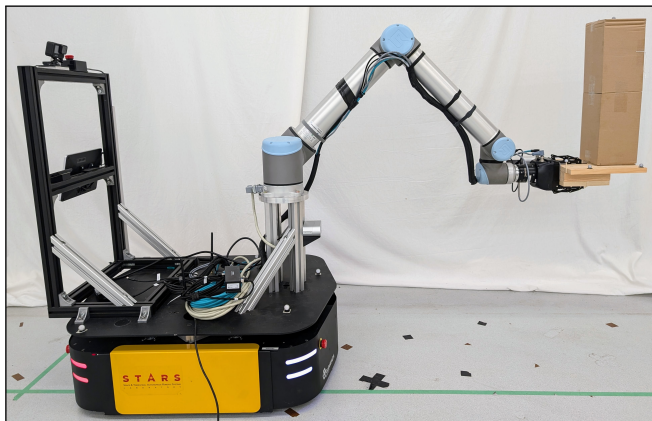


Fig. 1: The goal of this work is to move an object balanced on a tray to a desired position without dropping it, despite the inertial parameters of the object being uncertain. Here our mobile manipulator is balancing a tall box with uncertain contents. A video of our experiments is available at <http://tiny.cc/upright-robust>.

a desired EE position while satisfying constraints that ensure the balanced object does not move with respect to the tray (see Fig. 1). These balancing constraints depend on the geometric, frictional, and inertial properties of the object. The geometry of the object can in principle be estimated visually (e.g., using a camera), while frictional uncertainty can be reduced by using a high-friction material for the tray surface or by using a low friction coefficient in the planner [6]. However, the inertial properties can only be identified by moving the object around (see e.g. [7], [8]), which is time-consuming and could result in the object being dropped and damaged. Instead, we propose using *robust* constraints that successfully balance the object despite the presence of substantial inertial parameter uncertainty. Notably, we assume the CoM can be located at any height within the object, and that the inertia matrix can take any physically realizable value.

We focus on balancing a single object which can slide and is tall enough to tip over. We assume that the geometry of the object is known but the mass and inertia matrix are unknown, and that the CoM lies within a known polyhedral convex set. We use the object’s known geometry to constrain the set of possible inertial parameters. A set of inertial parameters can only be physically realized on a given shape if there exists a corresponding mass density function which is zero everywhere outside that shape [8]. We develop necessary conditions for the inertial parameters to be physically realizable on a bounding shape based on moment relaxations [9]. These realizability conditions allow us to verify that a planned trajectory does not violate the balancing constraints for *any* physically realizable value of the inertial parameters,

providing theoretical guarantees for the robustness of our planned trajectories. In summary, the contributions of this work are:

- a planner for nonprehensile object transportation that explicitly handles objects with uncertain CoMs, extending the framework from [6];
- a theoretical analysis of the balancing constraint satisfaction in the presence of a bounded CoM and any physically realizable inertia matrix, based on moment relaxations [9];
- simulations and hardware experiments demonstrating that our proposed robust constraints successfully balance the object—despite using tall objects with high inertial parameter uncertainty—while baseline approaches drop the object;
- an open-source implementation of our planner, available at <https://github.com/utiasDSL/upright>.

II. RELATED WORK

The waiter’s problem has been approached using a variety of methods including offline planning [5], [10]–[12], online planning (i.e., model predictive control) [6], [13], and reactive control [14]–[17]. Few of these approaches address inertial parameter uncertainty in the balanced objects. One possible approach is to simulate the motion of a pendulum with the EE, which naturally minimizes lateral forces acting on the balanced object without explicitly modelling it. However, so far this approach has only been used to minimize slosh when transporting liquids [14] and [15] rather than (uncertain) rigid bodies. Another approach is [12], which develops a robust planner for the waiter’s problem based on reachability analysis, with parameter uncertainty represented using polynomial zonotopes. In contrast to our work, [12] focuses on small amounts of uncertainty (e.g., a 5% mass and inertia reduction) in both the balanced objects and the links of the robot. The resulting trajectories are also quite slow, with negligible inertial acceleration (i.e., quasistatic). Instead, we achieve fast and dynamic motion with tall objects under high parameter uncertainty (i.e., CoMs located at any height in the object and *any* realizable inertia matrix), but we assume that uncertainty in the robot model is negligible (i.e., we use a well-calibrated industrial robot).

Our formulation of robust balancing constraints draws inspiration from legged robot balance control [18]–[21]. Indeed, the task of balancing an object on a tray is quite similar to balancing a legged robot represented with a reduced-order model, which uses the centroidal dynamics of the robot (i.e., the dynamics of a rigid body). In [19]–[21], the CoM of the robot is assumed to be uncertain and motions are generated that keep the robot balanced for any possible CoM value in a polyhedral set. In particular, we follow a similar approach to [21] for handling polyhedral CoM uncertainty by enforcing balancing constraints corresponding to a CoM located at each vertex of the set, and demonstrate its effectiveness for the waiter’s problem. In contrast to these approaches, however, we are also interested in modelling and handling uncertainty in the inertia matrix. While the CoM can reasonably and

intuitively be assumed to live in some convex polyhedral set, the inertia matrix is more complicated. When considering the inertia matrix, the set of physically realizable inertial parameters is *spectrahedral* (i.e., it can be represented using linear matrix inequalities (LMIs)) rather than polyhedral, as discussed in [8]. We develop necessary conditions for the inertial parameters to be physically realizable on a bounding shape, based on moment relaxations [9], which we use as constraints in a semidefinite program (SDP) to verify that our planned trajectories do not violate any balancing constraints despite inertial parameter uncertainty. Moment relaxations (i.e., Lasserre’s hierarchy) have previously been applied in robotics for tasks like certifiable localization [22] and trajectory planning [23], but not to bounds on the inertial parameters of a rigid body.

III. MODELLING

We start by defining notation and presenting the models of the robot and balanced object.

A. Notation

We denote the set of real numbers as \mathbb{R} , the non-negative reals as \mathbb{R}_+ , the non-negative integers as \mathbb{N} , the $n \times n$ symmetric matrices as \mathbb{S}^n , the symmetric positive semidefinite matrices as \mathbb{S}_+^n , and the symmetric positive definite matrices as \mathbb{S}_{++}^n . The notation $\mathbf{A} \preceq \mathbf{B}$ means that $\mathbf{B} - \mathbf{A} \in \mathbb{S}_+^n$, while \leq denotes entry-wise inequality. The $n \times n$ identity matrix is denoted $\mathbf{1}_n$. Finally, we use $\text{diag}(\cdot)$ to construct (block) diagonal matrices.

B. Robot Model

As in [6], we consider a velocity-controlled mobile manipulator with state $\mathbf{x} = [\mathbf{q}^T, \boldsymbol{\nu}^T, \dot{\boldsymbol{\nu}}^T]^T \in \mathbb{R}^{n_x}$, where \mathbf{q} is the generalized position, which includes the planar pose of the mobile base and the arm’s joint angles, and $\boldsymbol{\nu}$ is the generalized velocity. The input $\mathbf{u} \in \mathbb{R}^{n_u}$ is the generalized jerk. We use a kinematic model, which we represent generically as

$$\dot{\mathbf{x}} = \mathbf{a}(\mathbf{x}) + \mathbf{B}(\mathbf{x})\mathbf{u},$$

with $\mathbf{a}(\mathbf{x}) \in \mathbb{R}^{n_x}$ and $\mathbf{B}(\mathbf{x}) \in \mathbb{R}^{n_x \times n_u}$. Though the actual commands sent to the robot are velocities, including acceleration and jerk in the model allows us to reason about the balancing constraints and encourage smoothness.

C. Object Model

We model the balanced object as a rigid body subject to the Newton-Euler equations

$$\mathbf{w}_C = \mathbf{w}_{GI}, \quad (1)$$

where \mathbf{w}_C is the contact wrench (CW) and \mathbf{w}_{GI} is the gravito-inertial wrench (GIW). Expressed in a frame attached to the EE, we have

$$\mathbf{w}_{GI} = \boldsymbol{\Xi}\boldsymbol{\eta} - \text{ad}(\boldsymbol{\xi})^T \boldsymbol{\Xi}\boldsymbol{\xi}, \quad (2)$$

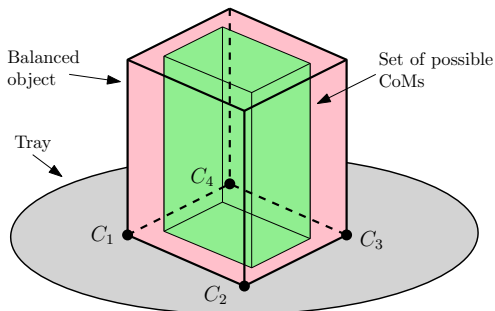


Fig. 2: A box (red) balanced on a tray, with four contact points C_1 – C_4 located at the vertices of the base. We assume that the box’s center of mass (CoM) is not known exactly, but rather only known to lie inside some polyhedral set (green).

where $\Xi \in \mathbb{S}_+^6$ is the object’s spatial mass matrix, $\xi = [\omega^T, v^T]^T$ is the spatial velocity with angular component $\omega \in \mathbb{R}^3$ and linear component $v \in \mathbb{R}^3$,

$$\text{ad}(\xi) \triangleq \begin{bmatrix} \omega^\times & \mathbf{0} \\ v^\times & \omega^\times \end{bmatrix}$$

is the adjoint of ξ with $(\cdot)^\times$ forming a skew-symmetric matrix such that $a^\times b = a \times b$ for any $a, b \in \mathbb{R}^3$, and $\eta = [\dot{v}^T - g^T, \dot{\omega}^T]^T$ is the difference between the spatial acceleration $\dot{\xi} = [\dot{\omega}^T, \dot{v}^T]^T$ and the gravitational acceleration $g \in \mathbb{R}^3$ (in the EE frame). The mass matrix is defined as

$$\Xi \triangleq \begin{bmatrix} \mathbf{I} & mc^\times \\ -mc^\times & m\mathbf{1}_3 \end{bmatrix},$$

where m is the object’s mass, c is the position of the object’s CoM, and \mathbf{I} is its inertia matrix expressed with respect to the origin of the EE frame.

IV. ROBUST BALANCING CONSTRAINTS

To control the interaction between the EE and balanced objects in the most general case, we would need to reason about the hybrid dynamics resulting from different contact modes (sticking, sliding, no contact, etc.). Instead, our approach is to enforce constraints that keep the system in a single mode (sticking); that is, we constrain the robot’s motion so that the balanced objects do not move with respect to the EE. This is known as a *dynamic grasp* [24].

A. Contact Force Constraints

We can ensure an object sticks to the EE by including all contact forces directly into the motion planner and constraining the solution to be consistent with the desired (sticking) dynamics. Optimizing over a set of contact forces to handle a given wrench is known as the *force optimization problem* [25]. Suppose there are n_c contact points $\{C_i\}_{i=1}^{n_c}$ between the object and tray (see Fig. 2), with corresponding contact forces $\{f_i\}_{i=1}^{n_c}$. By Coulomb’s law, each contact force $f_i \in \mathbb{R}^3$ must lie inside its friction cone, which we linearize to obtain the set of constraints $F_i f_i \leq \mathbf{0}$, where

$$F_i = \begin{bmatrix} 0 & 0 & -1 \\ 1 & 1 & -\mu_i \\ 1 & -1 & -\mu_i \\ -1 & 1 & -\mu_i \\ -1 & -1 & -\mu_i \end{bmatrix} [\hat{t}_{i1} \quad \hat{t}_{i2} \quad \hat{n}_i]^T,$$

with friction coefficient μ_i , contact normal \hat{n}_i , and orthogonal contact tangent directions \hat{t}_{i1} and \hat{t}_{i2} . Letting $\zeta = [f_1^T, \dots, f_{n_c}^T]^T$, we can write the linearized friction cone constraints for all n_c contact forces in matrix form as

$$F\zeta \leq \mathbf{0}, \quad (3)$$

where $F = \text{diag}(F_1, \dots, F_{n_c})$. The CW on the object is

$$w_C \triangleq \begin{bmatrix} \tau_C \\ f_C \end{bmatrix} = \sum_{i=1}^{n_c} G_i f_i, \quad (4)$$

where τ_C and f_C are the total contact torque and force and

$$G_i = \begin{bmatrix} r_i^\times \\ \mathbf{1}_3 \end{bmatrix}$$

is the i th contact Jacobian with r_i the location of C_i with respect to the EE. The object is successfully balanced at a given time instant if a set of contact forces can be found satisfying (1)–(4). This approach can handle any number of (possibly non-coplanar) contact points, with surface contacts represented as polygons with a contact point at each vertex.

The set \mathcal{W}_C of all possible contact wrenches is known as the *contact wrench cone* (CWC) [18], which is a polyhedral convex cone (PCC) containing all CWs that can be produced by feasible contact forces. We have $\mathcal{W}_C = \{G\zeta \mid F\zeta \leq \mathbf{0}\}$, where $G = [G_1, \dots, G_{n_c}]$ is known as the *grasp matrix*. From (1) we see that we must have $w_{GI} \in \mathcal{W}_C$ for the object to be balanced.

B. Robustness to Inertial Parameter Uncertainty

Let $\theta = [m, mc^T, \text{vech}(\mathbf{I})^T]^T \in \mathbb{R}^{10}$ be the inertial parameter vector for the balanced object, where $\text{vech}(\mathbf{I}) \in \mathbb{R}^6$ is the *half-vectorization* of \mathbf{I} [7]. Furthermore, let us assume that the exact value of θ is unknown, but that it lies inside a set Θ . Since w_{GI} is linear in θ [7], we can write the set of possible GIWs under inertial parameter uncertainty as

$$\mathcal{W}_{GI}(\xi, \eta) = \{Y(\xi, \eta)\theta \mid \theta \in \Theta\} \quad (5)$$

where $Y(\xi, \eta) \in \mathbb{R}^{6 \times 10}$ is known as the *regressor matrix*, which is linear in η and quadratic in ξ . To ensure the balancing constraints are satisfied for any possible $\theta \in \Theta$, we want to generate EE motions (ξ, η) that satisfy

$$\mathcal{W}_{GI}(\xi, \eta) \subseteq \mathcal{W}_C \quad (6)$$

at all timesteps. More concretely, (6) is satisfied if and only if, for each $\theta \in \Theta$, there exists a set of contact forces ζ satisfying $Y(\xi, \eta)\theta = G\zeta$ and $F\zeta \leq \mathbf{0}$.

We can enforce (6) using only constraints on the extreme points $\text{ex}(\Theta)$ of Θ . To see this, observe that since \mathcal{W}_C is convex, any convex combination of points in \mathcal{W}_C also lies in \mathcal{W}_C . And since any $\theta \in \Theta$ is a convex combination of points in $\text{ex}(\Theta)$, it follows that $Y(\xi, \eta)\theta \in \mathcal{W}_C$ for any $\theta \in \Theta$ as long as $Y(\xi, \eta)\theta \in \mathcal{W}_C$ for all $\theta \in \text{ex}(\Theta)$.

Furthermore, it turns out that we can ignore the value of the object’s mass when balancing a single object. To see this, suppose the true inertial parameter vector is $\theta = [m, mc^T, \text{vech}(\mathbf{I})^T]^T \in \Theta$. Since \mathcal{W}_C is a convex cone

and $m > 0$, it follows that $\mathbf{Y}(\boldsymbol{\xi}, \boldsymbol{\eta})\boldsymbol{\theta} \in \mathcal{W}_C$ if and only if $\mathbf{Y}(\boldsymbol{\xi}, \boldsymbol{\eta})\hat{\boldsymbol{\theta}} \in \mathcal{W}_C$, where $\hat{\boldsymbol{\theta}} \triangleq \boldsymbol{\theta}/m$ is the *mass-normalized* parameter vector.¹ In other words, for any $\boldsymbol{\theta} \in \Theta$, we can always instead use $\hat{\boldsymbol{\theta}}$ to enforce the balancing constraints, which is independent of the true mass. This result holds for any object that is not in contact with any others (except of course the tray). However, when multiple objects are in contact with each, the force transmitted between them depends on their relative masses, so we can no longer ignore them.

Finally, we will also ignore uncertainty in the inertia matrix *while planning* trajectories, as it would be expensive to enforce the semidefinite constraint required for physical realizability [8]. Instead, we will check our trajectories *after planning* to verify that the balancing constraints are satisfied for any physically realizable inertial parameters—our experiments suggest that handling large uncertainty in the CoM gives us enough robustness to handle any physically realizable inertia matrix as well. We will return to the analysis of physically realizable inertial parameters in Sec. VI. For now, since we are ignoring uncertainty in the mass and inertia matrix, we are left with uncertainty in the CoM. Similar to [21], our approach therefore is to assume that \mathbf{c} belongs to a known polyhedral set \mathcal{C} with n_v vertices (see Fig. 2) and enforcing balancing constraints for n_v objects, which differ only in that the i th object has CoM located at the i th vertex of the CoM uncertainty set. This is equivalent to enforcing (6).

V. PLANNING FOR ROBUST BALANCING

Our goal is to generate a state-input trajectory for our robot that satisfies the robust balancing constraints developed in the previous section. We formulate the motion planning problem as a constrained optimal control problem (OCP), similar to the formulation in [6]. In contrast to [6], however, which solves the OCP online in a model predictive control framework, we solve it once offline with a longer time horizon and then track the resulting optimal trajectory; we found this approach to be more reliable in our real-world experiments with tall, uncertain balanced objects. The trajectories $\mathbf{x}(t)$, $\mathbf{u}(t)$, and $\boldsymbol{\zeta}(t)$ are optimized over a duration T by solving a nonlinear optimization problem. Suppressing the time dependencies, the problem is

$$\begin{aligned} & \underset{\mathbf{x}, \mathbf{u}, \boldsymbol{\zeta}}{\operatorname{argmin}} && \frac{1}{2} \int_0^T \ell(\mathbf{x}, \mathbf{u}) dt \\ \text{subject to} &&& \dot{\mathbf{x}} = \mathbf{a}(\mathbf{x}) + \mathbf{B}(\mathbf{x})\mathbf{u} && \text{(robot model)} \\ &&& \mathcal{W}_{\text{GI}}(\mathbf{x}) \subseteq \mathcal{W}_C && \text{(balancing)} \\ &&& \mathbf{x} \leq \mathbf{x} \leq \bar{\mathbf{x}} && \text{(state limits)} \\ &&& \mathbf{u} \leq \mathbf{u} \leq \bar{\mathbf{u}} && \text{(input limits)} \\ &&& \boldsymbol{\varphi}(\mathbf{x}_f) = \mathbf{0} && \text{(terminal constraint)} \end{aligned} \quad (7)$$

where the stage cost is

$$\ell(\mathbf{x}, \mathbf{u}) = \|\Delta \mathbf{r}(\mathbf{x})\|_{\mathbf{W}_r}^2 + \|\mathbf{x}\|_{\mathbf{W}_x}^2 + \|\mathbf{u}\|_{\mathbf{W}_u}^2,$$

¹The mass-normalized inertia matrix $\hat{\mathbf{I}} \triangleq \mathbf{I}/m$ is known as the *gyration matrix*, which encodes the *spread* of the mass distribution but not its magnitude.

with $\|\cdot\|_{\mathbf{W}}^2 = (\cdot)^T \mathbf{W}(\cdot)$ for weight matrix \mathbf{W} , and $\Delta \mathbf{r}(\mathbf{x}) = \mathbf{r}_d - \mathbf{r}_e(\mathbf{x})$ is the EE position error between the desired position \mathbf{r}_d and the current position $\mathbf{r}_e(\mathbf{x})$. The balancing constraints implicitly depend on the contact forces $\boldsymbol{\zeta}$, and we have expressed \mathcal{W}_{GI} as a function of the joint state \mathbf{x} via forward kinematics. The terminal constraint $\boldsymbol{\varphi}(\mathbf{x}_f) = [\Delta \mathbf{r}(\mathbf{x}_f)^T, \boldsymbol{\nu}_f^T, \dot{\boldsymbol{\nu}}_f^T]^T = \mathbf{0}$ acts only the final state $\mathbf{x}_f \triangleq \mathbf{x}(T)$ and steers the trajectory toward a stationary state with no position error.

We solve (7) by discretizing the planning horizon T with a fixed timestep Δt and using sequential quadratic programming (SQP) via the open-source framework OCS2 [26] and quadratic programming solver HPIPM [27], with required Jacobians computed using automatic differentiation. We use the Gauss-Newton approximation for the Hessian of the cost and we soften the state constraints: given a generic state constraint $g(\mathbf{x}) \geq 0$, we add a slack variable $s \geq 0$ to relax the constraint to $g(\mathbf{x}) + s \geq 0$, and the L_2 penalty $w_s s^2$ is added to the cost with weight $w_s > 0$. Finally, like [6], we plan while assuming that there is *zero* contact friction between the tray and balanced object. This provides robustness to uncertain friction and other disturbances while also reducing the computational cost of solving (7), since each contact force variable need only be represented by a single non-negative scalar representing the normal force (see [6] for more details).

Once we have solved (7) to obtain the planned optimal trajectory $\mathbf{x}_d(t) = [\mathbf{q}_d^T(t), \boldsymbol{\nu}_d^T(t), \dot{\boldsymbol{\nu}}_d^T(t)]^T$, we need to track it online. At each control timestep, we generate the commanded velocity $\boldsymbol{\nu}_{\text{cmd}}$ using the simple affine control law $\boldsymbol{\nu}_{\text{cmd}} = \mathbf{K}_p(\mathbf{q}_d - \mathbf{q}) + \boldsymbol{\nu}_d$, where $\mathbf{K}_p \in \mathbb{S}_{++}^9$ is a gain matrix.

VI. VERIFYING BALANCING CONSTRAINT SATISFACTION

Let us now consider uncertainty in the inertia matrix. We want to show that our choice to ignore inertia matrix uncertainty in the planner is justified; that is, given a trajectory, we want to verify that the balancing constraints are not violated for *any* realizable value of the inertia matrix. In this section we develop an SDP to determine an upper-bound on the maximum constraint violation given the uncertain inertial parameters and bounding shape for the object.

A. Double Description of the Contact Wrench Cone

To begin, it will be helpful to express the CWC differently than in Sec. IV. We will use the fact that any PCC \mathcal{P} can be described using either the *face* or *span* form:

$$\begin{aligned} \mathcal{P} &= \operatorname{face}(\mathbf{U}) = \{\mathbf{y} \mid \mathbf{U}\mathbf{y} \leq \mathbf{0}\} \\ &= \operatorname{span}(\mathbf{V}) = \{\mathbf{V}\mathbf{z} \mid \mathbf{z} \geq \mathbf{0}\}, \end{aligned}$$

which is referred to as a *double description* of \mathcal{P} . Following [28], we use the superscript $(\cdot)^F$ to denote conversion from span to face form, such that $\operatorname{face}(\mathbf{U}^F) = \operatorname{span}(\mathbf{U})$, and we use $(\cdot)^S$ to denote the conversion from face to span form. We perform the actual numerical conversions using the `cdd` library [29].

Following [18], we build the face form of the CWC. First, notice that (3) describes a PCC $\operatorname{face}(\mathbf{F})$. Converting (3) to span form, we have $\mathcal{W}_C = \{\mathbf{G}\mathbf{F}^S \mathbf{z} \mid \mathbf{z} \geq \mathbf{0}\}$. Next,

letting $\mathbf{H} = (\mathbf{GF}^S)^F \in \mathbb{R}^{n_h \times 6}$, we have the face form of the CWC $\mathcal{W}_C = \{\mathbf{w} \in \mathbb{R}^6 \mid \mathbf{H}\mathbf{w} \leq \mathbf{0}\}$. This form allows us to write the robust balancing constraints (6) as

$$\mathbf{H}\mathbf{Y}(\boldsymbol{\xi}, \boldsymbol{\eta})\boldsymbol{\theta} \leq \mathbf{0} \quad \forall \boldsymbol{\theta} \in \Theta. \quad (8)$$

Let \mathbf{h}_i^T be the i th row of \mathbf{H} . Then we can rewrite the constraint (8) as a set of inner optimization problems

$$\left(\max_{\boldsymbol{\theta} \in \Theta} \mathbf{h}_i^T \mathbf{Y}(\boldsymbol{\xi}, \boldsymbol{\eta})\boldsymbol{\theta} \right) \leq 0, \quad (9)$$

with one problem for each of the n_h rows. This inequality form of the balancing constraints will allow us to solve for the worst-case value of each constraint. However, we first need to determine appropriate bounds on the set Θ .

B. Moment Relaxations

To determine bounds on the set of physically realizable inertial parameters, we will make use of some mathematical machinery for the *moment problem*, which asks when a sequence corresponds to the moments of some Borel measure. In particular, we will make use of SDP relaxations for the moment problem (*moment relaxations*), which we briskly summarize here from [9]. Define $\mathbb{N}_d^n = \{\boldsymbol{\alpha} \in \mathbb{N}^n \mid \sum_{i=1}^n \alpha_i \leq d\}$. Let $\mathbf{r} \in \mathbb{R}^n$ be a point and let $\boldsymbol{\alpha} \in \mathbb{N}_d^n$ be a vector of exponents applied elementwise, such that $\mathbf{r}^\boldsymbol{\alpha} = r_1^{\alpha_1} \dots r_n^{\alpha_n}$, and let $f: \mathbb{R}^n \rightarrow \mathbb{R}$ be a polynomial of degree at most d . Then we can write $f(\mathbf{r}) = \sum_{\boldsymbol{\alpha} \in \mathbb{N}_d^n} f_\boldsymbol{\alpha} \mathbf{r}^\boldsymbol{\alpha} = \mathbf{f}^T \mathbf{b}_d(\mathbf{r})$, where $\mathbf{f} = \{f_\boldsymbol{\alpha}\} \in \mathbb{R}^{s(d)}$ is the vector of the polynomial's coefficients with size $s(d) \triangleq \binom{n+d}{d}$ and $\mathbf{b}_d(\mathbf{r}) = [1, r_1, \dots, r_n, r_1^2, r_1 r_2, \dots, r_n^d] \in \mathbb{R}^{s(d)}$ is the basis vector for polynomials of degree at most d in graded lexicographical order. Next, suppose we have a vector $\mathbf{z} = \{z_\boldsymbol{\alpha}\} \in \mathbb{R}^{s(d)}$. The *Riesz functional* associated with \mathbf{z} is $L_{\mathbf{z}}(f) = \sum_{\boldsymbol{\alpha} \in \mathbb{N}_d^n} f_\boldsymbol{\alpha} z_\boldsymbol{\alpha}$, which maps a polynomial $f: \mathbb{R}^n \rightarrow \mathbb{R}$ of degree d to a scalar value. Further suppose we have a vector $\mathbf{y} \in \mathbb{R}^{s(2d)}$ and a polynomial $p: \mathbb{R}^n \rightarrow \mathbb{R}$ of degree $2d$ with coefficients $\mathbf{p} = \{p_\boldsymbol{\gamma}\} \in \mathbb{R}^{s(2d)}$. The d th-order *moment matrix* associated with \mathbf{y} is

$$\mathbf{M}_d(\mathbf{y}) = L_{\mathbf{y}}(\mathbf{b}_d(\mathbf{r})\mathbf{b}_d(\mathbf{r})^T) \in \mathbb{R}^{s(d) \times s(d)},$$

where $L_{\mathbf{y}}$ is applied elementwise to each element of the matrix $\mathbf{b}_d(\mathbf{r})\mathbf{b}_d(\mathbf{r})^T$, such that the element $\mathbf{r}^\boldsymbol{\alpha} \mathbf{r}^\boldsymbol{\beta} = \mathbf{r}^{\boldsymbol{\alpha}+\boldsymbol{\beta}}$, with $\boldsymbol{\alpha}, \boldsymbol{\beta} \in \mathbb{N}_d^n$, is mapped to the value $y_{\boldsymbol{\alpha}+\boldsymbol{\beta}}$. In addition, the *localizing matrix* associated with p and \mathbf{y} is $\mathbf{M}_d(p\mathbf{y}) = L_{\mathbf{y}}(p\mathbf{b}_d(\mathbf{r})\mathbf{b}_d(\mathbf{r})^T)$. For example, suppose $n = 2$, $d = 1$, and $p(\mathbf{r}) = a - r_1$ for some constant a . Then

$$\begin{aligned} \mathbf{M}_d(p\mathbf{y}) &= L_{\mathbf{y}}(p\mathbf{b}_d(\mathbf{r})\mathbf{b}_d(\mathbf{r})^T) \\ &= L_{\mathbf{y}} \left((a - r_1) \begin{bmatrix} 1 & r_1 & r_2 \\ r_1 & r_1^2 & r_1 r_2 \\ r_2 & r_1 r_2 & r_2^2 \end{bmatrix} \right) \\ &= \begin{bmatrix} ay_{00} - y_{10} & ay_{10} - y_{20} & ay_{01} - y_{11} \\ ay_{10} - y_{20} & ay_{20} - y_{30} & ay_{11} - y_{21} \\ ay_{01} - y_{11} & ay_{11} - y_{21} & ay_{02} - y_{12} \end{bmatrix}. \end{aligned}$$

Suppose we want to determine if a given sequence $\mathbf{y} \in \mathbb{R}^{s(2d)}$, known as a *truncated moment sequence (TMS)*,

represents the moments of some Borel measure μ supported in a compact semialgebraic set $\mathcal{K} = \{\mathbf{r} \in \mathbb{R}^n \mid p_j(\mathbf{r}) \geq 0, j = 1, \dots, n_p\}$, where each $p_j(\mathbf{r})$ is a polynomial with degree $2v_j$ (even) or $2v_j - 1$ (odd). That is, we want to know if there exists $\mu: \mathbb{R}^n \rightarrow \mathbb{R}_+$ such that

$$\mathbf{M}_d(\mathbf{y}) = \int_{\mathcal{K}} \mathbf{b}_d(\mathbf{r})\mathbf{b}_d(\mathbf{r})^T d\mu(\mathbf{r}),$$

which is known as the *truncated K-moment problem (TKMP)*. Define $p_0(\mathbf{r}) = 1$ with $v_0 = 0$. Then a necessary condition for such a measure to exist (see Theorem 3.8 of [9]) is that for any $r \geq d$, we can extend $\mathbf{y} \in \mathbb{R}^{s(2d)}$ to $\tilde{\mathbf{y}} \in \mathbb{R}^{s(2r)}$ such that

$$\mathbf{M}_{r-v_j}(p_j \tilde{\mathbf{y}}) \succcurlyeq \mathbf{0}, \quad j = 0, \dots, n_p. \quad (10)$$

The moment constraints (10) become tighter as r increases, which can be used to form a hierarchy of SDP relaxations for the TKMP.

C. Worst-Case Balancing Constraints

Let us now apply the TKMP machinery to the problem of physically realizable inertial parameters. Let $n = 3$ and $d = 1$. Then the TMS $\mathbf{y} \in \mathbb{R}^{10}$ and the associated moment matrix $\mathbf{M}_1(\mathbf{y})$ can be used to represent the inertial parameters of a rigid body, with the relationship

$$\mathbf{M}_1(\mathbf{y}) = \begin{bmatrix} m & m\mathbf{c}^T \\ m\mathbf{c} & \mathbf{S} \end{bmatrix}, \quad (11)$$

where $\mathbf{S} = (1/2)\text{tr}(\mathbf{I})\mathbf{1}_3 - \mathbf{I}$ is known as the *second moment matrix* [8].² We want to constrain the inertial parameters to correspond to a mass density $\rho: \mathbb{R}^3 \rightarrow \mathbb{R}_+$ supported entirely in a compact bounding shape $\mathcal{K} = \{\mathbf{r} \in \mathbb{R}^3 \mid p_j(\mathbf{r}) \geq 0, j = 1, \dots, n_p\}$ that contains the balanced object, such that

$$\mathbf{M}_1(\mathbf{y}) = \int_{\mathcal{K}} \mathbf{b}_1(\mathbf{r})\mathbf{b}_1(\mathbf{r})^T d\rho(\mathbf{r}).$$

For simplicity we assume our bounding shape is a convex polyhedron, so $v_j = 1$ for each $j = 1, \dots, n_p$, and again we take $p_0(\mathbf{r}) = 1$ with $v_0 = 0$. Given an EE trajectory, we want to determine if any realizable value of the inertial parameters would violate the balancing constraints (9) at any time. In particular, we would like to know if the optimal value of

$$\max_{\boldsymbol{\theta} \in \Theta} \mathbf{h}_i^T \mathbf{Y}(\boldsymbol{\xi}, \boldsymbol{\eta})\boldsymbol{\theta} \quad (12)$$

is positive for any row \mathbf{h}_i^T of \mathbf{H} at any time instant of the trajectory. Using the conditions (10) with $r = 2$, the problem (12) can be relaxed to the SDP

$$\begin{aligned} &\max_{\boldsymbol{\theta}, \tilde{\mathbf{y}}} \mathbf{h}_i^T \mathbf{Y}(\boldsymbol{\xi}, \boldsymbol{\eta})\boldsymbol{\theta} \\ &\text{subject to} \quad \mathbf{M}_1(\tilde{\mathbf{y}}) = \begin{bmatrix} 1 & \mathbf{c}(\boldsymbol{\theta})^T \\ \mathbf{c}(\boldsymbol{\theta}) & \mathbf{S}(\boldsymbol{\theta}) \end{bmatrix}, \\ &\quad \mathbf{M}_{2-v_j}(p_j \tilde{\mathbf{y}}) \succcurlyeq \mathbf{0}, \quad j = 0, \dots, n_p, \\ &\quad \mathbf{c}(\boldsymbol{\theta}) \in \mathcal{C}, \end{aligned} \quad (13)$$

²A permuted version of (11), known as the *pseudo-inertia matrix*, is the more common form in the robot dynamics literature (see e.g. [8]), but here we maintain consistency with the TKMP literature [9].

where $\tilde{\mathbf{y}} \in \mathbb{R}^{20}$ is an extended TMS, we have constrained the CoM \mathbf{c} to be located within some convex polyhedron $\mathcal{C} \subset \mathcal{K}$, and we have fixed $m = 1$ since the balancing constraints are independent of mass for a single object. We have also made the dependencies on the decision variable θ explicit for clarity; note that \mathbf{S} and \mathbf{c} depend linearly on θ .

Since (13) is a relaxation of (12), its optimal value is an upper bound on the maximum possible violation for each balancing constraint. Notably, (13) accounts for all possible values of the inertia matrix. We verify that a planned trajectories is robust to inertial parameter uncertainty by solving (10) pointwise at a fixed frequency along the trajectory. If the optimal value of (13) is always non-positive, then the constraint is never violated. Furthermore, we can verify frictional robustness at the same time by constructing \mathcal{W}_C and thus \mathbf{H} with low friction coefficients; if the constraint is never violated, then any combination of larger friction coefficients and realizable inertial parameters will also satisfy the constraints.

One could also consider enforcing full realizability constraints directly in the planning problem (7) to ensure the planned trajectories are robust a priori. However, this would be computationally expensive and numerically challenging because of the LMI constraints required for physical realizability combined with the nonlinearity of the problem. We leave this for future work.

VII. SIMULATION EXPERIMENTS

We begin the evaluation of our proposed robust planning approach in simulation using the PyBullet simulator and a simulated version of our experimental platform, a 9-DOF mobile manipulator consisting of a Ridgeback mobile base and UR10 arm, shown in Fig. 1. In all experiments (simulated and real) we use $\Delta t = 0.1$ s, $T = 10$ s, and weights

$$\begin{aligned} \mathbf{W}_r &= \mathbf{1}_3, & \mathbf{W}_x &= \text{diag}(0\mathbf{1}_9, 10^{-1}\mathbf{1}_9, 10^{-2}\mathbf{1}_9), \\ \mathbf{W}_u &= 10^{-3}\mathbf{1}_9, & w_s &= 100. \end{aligned}$$

The state and input limits are

$$\bar{\mathbf{q}} = \begin{bmatrix} 10\mathbf{e}_3 \\ 2\pi\mathbf{e}_6 \end{bmatrix}, \bar{\mathbf{v}} = \begin{bmatrix} 1.1\mathbf{e}_2 \\ 2\mathbf{e}_3 \\ 3\mathbf{e}_4 \end{bmatrix}, \dot{\bar{\mathbf{v}}} = \begin{bmatrix} 2.5\mathbf{e}_2 \\ 1 \\ 10\mathbf{e}_6 \end{bmatrix}, \bar{\mathbf{u}} = \begin{bmatrix} 20\mathbf{e}_3 \\ 80\mathbf{e}_6 \end{bmatrix},$$

where $\bar{\mathbf{x}} = [\bar{\mathbf{q}}^T, \bar{\mathbf{v}}^T, \dot{\bar{\mathbf{v}}}^T]^T$, $\mathbf{x} = -\bar{\mathbf{x}}$, $\mathbf{u} = -\bar{\mathbf{u}}$, and \mathbf{e}_n denotes an n -dimensional vector of ones. The control gain is $\mathbf{K}_p = \mathbf{1}_9$. We use three SQP iterations per plan. All experiments are run on a standard laptop with eight Intel Xeon CPUs at 3 GHz and 16 GB of RAM.

We are interested in cases where the inertial parameters of the balanced object are uncertain and this uncertainty can result in task failures (i.e., the object is dropped) if the uncertainty is ignored. We use a tall box \mathcal{K} with a 15 cm \times 15 cm base and height h (see Fig. 3) as the balanced object. This object is tall relative to its support area and therefore prone to tipping over, particularly if the inertial parameters are not known exactly. Suppose we assume that the CoM can lie anywhere in a box \mathcal{C} with dimensions 12 cm \times 12 cm \times h , centered within \mathcal{K} ; that is, the CoM can be located *anywhere*

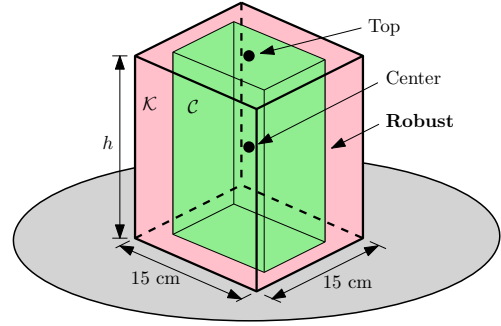


Fig. 3: We balance a cuboid-shaped object \mathcal{K} with an uncertain CoM contained in \mathcal{C} . We test three variations of the balancing constraints: assume the CoM is at the object's centroid (Center), assume it is centered at the top of the object (Top), and Robust, in which the controller enforces constraints to balance eight different objects, where each has its CoM at one of the vertices of \mathcal{C} .

in the object as long as it is at least 1.5 cm from the sides. The simulated friction coefficient between the box and tray is $\mu = 0.2$. We compare three sets of balancing constraints (again, see Fig. 3):

- **Center:** The CoM is located at the center of \mathcal{C} ;
- **Top:** The CoM is centered on the top face of \mathcal{C} ;
- **Robust:** A set of eight balancing constraints are used, corresponding to a CoM at each vertex of \mathcal{C} .

In all cases, the inertia matrix used in the planner is set to correspond to a uniform mass density. The first two constraint methods are baselines where we are not explicitly accounting for the uncertainty in the parameters. Intuitively, it is more difficult to balance an object with a higher CoM, so we may expect the Top constraints to be more successful than the Center constraints. In contrast to these baselines, our proposed Robust constraints explicitly handle uncertainty in the CoM.

We test three different trajectories corresponding to desired positions $\mathbf{r}_{d_1} = [-2, 1, 0]^T$, $\mathbf{r}_{d_2} = [0, 2, 0.25]^T$, and $\mathbf{r}_{d_3} = [2, 0, -0.25]^T$ (in meters), 15 different simulated CoM positions (one at the center of \mathcal{C} , eight at the vertices of \mathcal{C} , and six at the centers of the faces of \mathcal{C}), and three different values for the inertia matrix, computed as follows. We solve a convex optimization problem to find the diagonal inertia matrix about the CoM which corresponds to a set of point masses at the vertices of \mathcal{K} with the maximum smallest eigenvalue. This gives us a large realizable inertia matrix value \mathbf{I} ; we then also test with the smaller inertia values $0.5\mathbf{I}$ and $0.1\mathbf{I}$. The simulated mass is fixed to $m = 1$ kg. We test each of the 135 total combinations of trajectory, CoM, and inertia matrix for different object heights h and constraint methods.

The success rates for the simulations are shown in Fig. 4. The success rate is the percentage of runs (out of the 135 total per object) that successfully deliver the object to the goal without dropping it. The Top constraints are always successful for the lowest height of 30 cm, but there are an increasing number of failures as the object height increases. The Center constraints always produce fewer successful runs than the Top constraints. Finally, the proposed Robust constraints are always successful, with a maximum object displacement of only 2.6 cm across all runs.

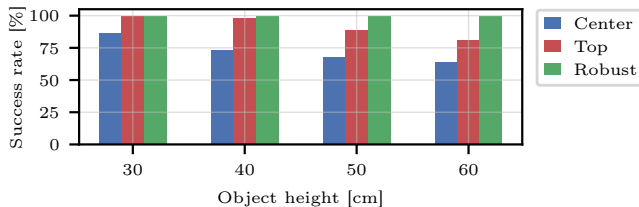


Fig. 4: Success rate of the of the different types of balancing constraints for all 135 combinations of desired positions, CoMs, and inertias for each object height and constraint method (1620 total runs). The Robust constraints always keep the object balanced, while the other constraint types result in an increasing number of failures as the object height increases.

TABLE I: Maximum constraint violation for each object height and balancing constraint method using the moment conditions for physical realizability. A negative value means that the constraints are never violated for any realizable inertial parameters, which is only the case using our proposed Robust constraints.

Height [cm]	Center	Top	Robust
30	2.31	3.71	-1.17
40	4.79	6.95	-0.99
50	7.92	10.57	-0.80
60	11.62	14.43	-0.59

While the results in Fig. 4 show that our proposed constraints are robust for *particular* combinations of CoM positions and inertia matrices, Table I shows the maximum possible balancing constraint violations for *any* realizable inertial parameter value, obtained by solving (13) at each point along the planned trajectory (discretized with a 10 ms interval). The Robust constraints have no violation for any possible value of the inertia matrix (while the Center and Top constraints always do), justifying our decision to ignore uncertainty in the inertia matrix within the planner. The average planning times for the Center, Top, and Robust constraint methods are 110 ms, 111 ms, and 326 ms, respectively; the time does not change substantially with object height.

Finally, recall that the simulated value of the friction coefficient between the tray and object is $\mu = 0.2$. This value does not impact the behavior of the planner because the planner assumes $\mu = 0$ and then tries to satisfy the softened balancing constraints approximately. However, the underlying value of μ can potentially affect the amount of constraint violation, since h_i in (13) depends on the friction coefficient. Interestingly, we evaluated the constraint violation for the robust constraints with $h = 60$ cm and $\mu = 0.1$ and found the maximum constraint violation to be the same as with $\mu = 0.2$, which suggests that the friction coefficient is not the limiting factor in balancing tall objects like those we are using here.

VIII. HARDWARE EXPERIMENTS

We also perform experiments on our real mobile manipulator balancing a cardboard box, as shown in Fig. 1. We test two heights of box, Box1 and Box2, each containing a bottle filled with sugar in one corner to offset the CoM (see Fig. 5). Box1 has a height of $h_1 = 28$ cm and a square base with side length 15 cm. Its total mass is 933 g, with the bottle contributing 722 g. Box2 is made of two stacked boxes attached together, with the top one containing the bottle. Its total mass is 1046 g and its height is $h_2 = 56$ cm; its base

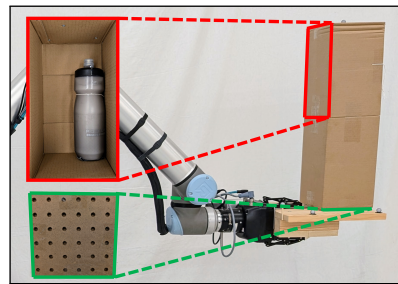


Fig. 5: Our balanced objects are boxes containing a bottle filled with sugar to offset the CoM and to make the task of balancing more difficult. One cannot tell how the box is packed (and therefore what its mass distribution is) just by looking at it. Box2 (shown on the right) consists of two boxes attached together; Box1 is a single box. A firm base board (green) is attached to the bottom box to provide a consistent contact area with the tray.

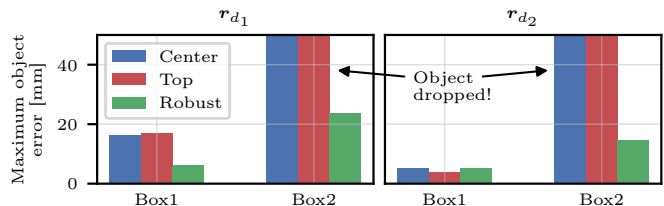


Fig. 6: Maximum object displacement error for the different constraint methods, desired positions, and box objects. The object displacement error is the maximum distance the object moves from its initial position relative to the tray. The errors are similar between each method with Box1 (the shorter box), but the Center and Top baselines fail with Box2 (the taller box), while the proposed Robust constraints successfully keep it balanced.

dimensions are the same as Box1. A rigid board is attached to the base of the boxes to ensure consistent contact with the tray (again, refer to Fig. 5). The friction coefficient between the boxes (with the attached base board) and the tray was experimentally measured to be $\mu = 0.29$. Position feedback is provided for the arm by joint encoders at 125 Hz and for the base by a Vicon motion capture system at 100 Hz. The laptop specifications and planner parameters are the same as in simulation. The control loop is run at the arm’s control frequency of 125 Hz.

We consider the scenario when the planner does not know how the box is packed, and therefore its inertial parameters are not known exactly. We again test the Center, Top, and Robust constraints using the desired positions r_{d1} and r_{d2} .³ The Robust constraints assume the CoM lies in the cuboid \mathcal{C} with dimensions $12 \text{ cm} \times 12 \text{ cm} \times h_i$, where $i = 1, 2$ corresponds to Box1 or Box2. We perform up to three runs of each combination of desired position and constraint method; if a given combination method fails before completing three runs, we stop to avoid extra damage to the balanced boxes. Each of the constraint methods successfully balanced Box1 for three runs, but only the Robust constraints were able to do so with Box2. The Center constraints failed immediately with r_{d1} , and completed one run of r_{d2} before dropping the box on the second run; the Top constraints failed immediately for both desired positions. The maximum object displacement errors are shown in Fig. 6. The Robust constraints produce

³We did not use the desired position r_{d3} because in that case if the box falls, it falls onto the robot, possibly causing damage.

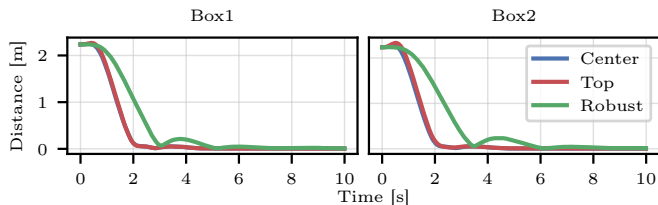


Fig. 7: Distance between the EE position and the desired position over time for desired position r_{d1} and each balancing constraint method. The trajectories with the Center and Top constraints, in which only a single CoM value is considered, are nearly the same. The Robust constraints result in slower convergence, but always successfully balance the object.

smaller errors with both Box1 and Box2; the Center and Top baselines obviously produce large errors with Box2 since the box was dropped.

The convergence of the EE to the desired position for r_{d1} is shown in Fig. 7. While the Center and Top constraint methods converge faster, this comes with the risk of failing to balance uncertain objects, especially taller ones like Box2. Furthermore, the Robust constraints still produce fast motion. With Box1, the planned trajectories subject to the Robust constraints achieve a maximum EE velocity of 1.27 m/s and a maximum EE acceleration of 1.17 m/s²; with Box2 they achieve 1.08 m/s and 0.87 m/s², respectively. The experiments can also be seen in the accompanying video.

IX. CONCLUSION

We present a planning framework for nonprehensile object transportation that is robust to uncertainty in the balanced object’s inertial parameters. In particular, we explicitly model and design robust constraints for uncertainty in the object’s CoM, and demonstrate that this successfully balances tall objects in simulation and on real hardware. We also use moment relaxations to develop conditions for the inertial parameters of the balanced object to be physically realizable, which allows us to determine if the balancing constraints would be violated for *any* possible value of the inertial parameters, including the inertia matrix, along the planned trajectories.

REFERENCES

- [1] F. G. Flores and A. Kecskeméthy, “Time-optimal path planning for the general waiter motion problem,” in *Advances in Mechanisms, Robotics and Design Education and Research*, 2013, pp. 189–203.
- [2] K. M. Lynch, “Nonprehensile robotic manipulation: Controllability and planning,” Ph.D., Carnegie Mellon University, 1996.
- [3] A. Heins and A. P. Schoellig, “Force push: Robust single-point pushing with force feedback,” *IEEE Robotics and Automation Letters*, vol. 9, no. 8, pp. 6856–6863, 2024.
- [4] F. Ruggiero, V. Lippiello, and B. Siciliano, “Nonprehensile dynamic manipulation: A survey,” *IEEE Robotics and Automation Letters*, vol. 3, no. 3, pp. 1711–1718, 2018.
- [5] Q.-C. Pham, S. Caron, P. Lertkultanon, and Y. Nakamura, “Admissible velocity propagation: Beyond quasi-static path planning for high-dimensional robots,” *Int. J. Robotics Research*, vol. 36, no. 1, pp. 44–67, 2017.
- [6] A. Heins and A. P. Schoellig, “Keep it upright: Model predictive control for nonprehensile object transportation with obstacle avoidance on a mobile manipulator,” *IEEE Robotics and Automation Letters*, vol. 8, no. 12, pp. 7986–7993, 2023.

- [7] S. Traversaro, S. Brossette, A. Escande, and F. Nori, “Identification of fully physical consistent inertial parameters using optimization on manifolds,” in *Proc. IEEE/RSJ Int. Conf. Intelligent Robots and Systems*, 2016, pp. 5446–5451.
- [8] P. M. Wensing, S. Kim, and J.-J. E. Slotine, “Linear matrix inequalities for physically consistent inertial parameter identification: A statistical perspective on the mass distribution,” *IEEE Robotics and Automation Letters*, vol. 3, no. 1, pp. 60–67, 2018.
- [9] J. B. Lasserre, *Moments, positive polynomials and their applications*. World Scientific, 2009.
- [10] C. Zhou, M. Lei, L. Zhao, Z. Wang, and Y. Zheng, “TOPP-MPC-based dual-arm dynamic collaborative manipulation for multi-object nonprehensile transportation,” in *Proc. IEEE Int. Conf. Robotics and Automation*, 2022, pp. 999–1005.
- [11] H. Gattringer, A. Müller, S. Weitzhofer, and M. Schörgenhuber, “Point to point time optimal handling of unmounted rigid objects and liquid-filled containers,” *Mechanism and Machine Theory*, vol. 184, p. 105286, 2023.
- [12] Z. Brei, J. Michaux, B. Zhang, P. Holmes, and R. Vasudevan, “Serving time: Real-time, safe motion planning and control for manipulation of unsecured objects,” *IEEE Robotics and Automation Letters*, vol. 9, no. 3, pp. 2383–2390, 2024.
- [13] M. Selvaggio, A. Garg, F. Ruggiero, G. Oriolo, and B. Siciliano, “Non-prehensile object transportation via model predictive non-sliding manipulation control,” *IEEE Trans. Control Systems Technology*, pp. 1–14, 2023.
- [14] L. Moriello, L. Biagiotti, C. Melchiorri, and A. Paoli, “Manipulating liquids with robots: A sloshing-free solution,” *Control Engineering Practice*, vol. 78, pp. 129–141, 2018.
- [15] R. I. C. Muchacho, R. Laha, L. F. C. Figueredo, and S. Haddadin, “A solution to slosh-free robot trajectory optimization,” in *Proc. IEEE/RSJ Int. Conf. Intelligent Robots and Systems*, 2022, pp. 223–230.
- [16] M. Selvaggio, J. Cacace, C. Pacchierotti, F. Ruggiero, and P. R. Giordano, “A shared-control teleoperation architecture for nonprehensile object transportation,” *IEEE Trans. Robotics*, vol. 38, no. 1, pp. 569–583, 2022.
- [17] R. Subburaman, M. Selvaggio, and F. Ruggiero, “A non-prehensile object transportation framework with adaptive tilting based on quadratic programming,” *IEEE Robotics and Automation Letters*, pp. 1–8, 2023.
- [18] S. Caron, Q. C. Pham, and Y. Nakamura, “Leveraging cone double description for multi-contact stability of humanoids with applications to statics and dynamics,” in *Proc. Robotics: Science and Systems*, 2015.
- [19] S. Caron and A. Kheddar, “Multi-contact walking pattern generation based on model preview control of 3D COM accelerations,” in *Proc. IEEE-RAS Int. Conf. Humanoid Robots*, 2016, pp. 550–557.
- [20] N. Giftsun, A. D. Prete, and F. Lamiroux, “Robustness to inertial parameter errors for legged robots balancing on level ground,” in *Proc. Int. Conf. Informatics in Control, Automation and Robotics*, 2017.
- [21] X. Jiang, W. Chi, Y. Zheng, S. Zhang, Y. Ling, J. Xu, and Z. Zhang, “Locomotion generation for quadruped robots on challenging terrains via quadratic programming,” *Autonomous Robots*, vol. 47, no. 1, pp. 51–76, 2023.
- [22] H. Yang and L. Carlone, “Certifiably optimal outlier-robust geometric perception: Semidefinite relaxations and scalable global optimization,” *IEEE Trans. Pattern Analysis and Machine Intelligence*, vol. 45, no. 3, pp. 2816–2834, 2023.
- [23] S. Kang, X. Xu, J. Sarva, L. Liang, and H. Yang, “Fast and certifiable trajectory optimization,” in *Proc. Workshop Algorithmic Foundations of Robotics*, 2024.
- [24] M. T. Mason and K. M. Lynch, “Dynamic manipulation,” in *Proc. IEEE/RSJ Int. Conf. Intelligent Robots and Systems*, 1993, pp. 152–159.
- [25] S. P. Boyd and B. Wegbreit, “Fast computation of optimal contact forces,” *IEEE Trans. Robotics*, vol. 23, no. 6, pp. 1117–1132, 2007.
- [26] “OCS2: An open source library for optimal control of switched systems.” [Online]. Available: <https://github.com/leggedrobotics/ocs2>
- [27] G. Frison and M. Diehl, “HPIPM: a high-performance quadratic programming framework for model predictive control,” *IFAC-PapersOnLine*, vol. 53, no. 2, pp. 6563–6569, 2020.
- [28] D. J. Balkcom and J. Trinkle, “Computing wrench cones for planar rigid body contact tasks,” *Int. J. Robotics Research*, vol. 21, no. 12, pp. 1053–1066, 2002.
- [29] K. Fukuda and A. Prodon, “Double description method revisited,” in *Proc. Combinatorics and Computer Science*, 1996, pp. 91–111.